Reduction and Oxidation of the *Arachno* Clusters $Fe_2(CO)_6(\mu\text{-}S)_2PtL_2$: Characterization of Distinct One- and Two-Electron Transfer Sites in Heteropolynuclear Compounds

Andre Morneau,[†] William E. Geiger,*[,†] Michael G. Richmond,*[,‡] Ming-Jaw Don,[‡] William H. Watson,*[,§] and Ante Nagl[§]

Department of Chemistry, University of Vermont, Burlington, Vermont 05405, Department of Chemistry, University of North Texas, Denton, Texas 76203, and Department of Chemistry, Texas Christian University, Fort Worth, Texas 76129

Received September 20, 2001

The reduction and oxidation properties of the *arachno*-heteropolynuclear metal clusters $Fe_2(CO)_6(\mu_3\text{-}S)_2PtL_2$, where L_2 = bipyridine (**1**), phenanthroline (**2**), diphenylphosphinoethane (**3**), diphenylphosphinoferrocene (**4**), or cyclooctadiene (**5**), have been examined by electrochemistry, IR spectroscopy, and ESR spectroscopy. An electron-transfer series involving up to five electrons is observed. The common characteristics are a fully reversible one-electron oxidation process to a monocation (in the range 0.13−0.38 V vs ferrocene) and a chemically reversible but electrochemically quasi-reversible two-electron reduction process (range −1.9 to −2.4 V). Complexes **1** and **2** also display a fully reversible one-electron reduction at a potential less negative (ca. −1.8 V) than the subsequent two-electron reduction. The LUMOs of **1** and **2** are predicted by EHMO calculations to be primarily π*-diimine based. Spectral data from the monoanions $\mathbf{1}^-$ and $\mathbf{2}^-$ are consistent with this orbital assignment: very small shifts of the metal−carbonyl IR frequencies (ca. −13 cm^{-1}) from those of the neutral complexes are observed, and the ^{195}Pt hyperfine splitting in ESR spectra is very small compared to that expected for a metal-localized radical. The two-electron reductions forming, e.g., $\mathbf{1}^{3-}$ or $\mathbf{3}^{2-}$, appear to involve the Fe_2S_2 moiety and most likely are concomitant with breaking and making of an Fe−Fe bond. Carbonyl IR energies are lowered in excess of 100 cm^{-1} in the two-electron reduction. The oxidation processes appear to be localized on the $Fe_2(CO)_6S_2$ fragment, with IR shifts of 46−76 cm^{-1} for $\mathbf{1}^+$−$\mathbf{5}^+$ and small ^{195}Pt hyperfine splittings. X-ray crystal structures are reported for **2** and **5**.

Introduction

Electron-transfer reactions are relevant to the chemical and physical properties of a range of hetero-polynuclear compounds, including those showing activity as catalysts[1−3]or multielectron-transfer agents,[4] and those being considered as models for metalloproteins.[5−7] When dissimilar electron-transfer sites exist in a polynuclear compound, the interaction between those sites determines the mixed-valent properties and influences the spectra and reactivities of the electron-transfer products.[8−10] Electrochemistry and spectroelectrochemistry are among the most powerful techniques for examining metal−metal (or, more generally, site−site) interactions in such compounds.[11] We report here on the electron-transfer properties of a series of complexes containing $Fe_2(CO)_6$ and PtL_2 moieties linked by a bridging $(\mu_3\text{-}S)_2$ group in which a bidentete ligand L_2 may be either electron-donating or electron-accepting. Electrochemical and spectroscopic data show that these complexes support an extensive electron-transfer series involving up to five electrons in which the location of the first reduction site is determined by the identity of the bidentete ligand bonded to platinum. Each of the complexes also exhibits a two-electron reduction process and a one-electron oxidation process involving predominantly the diiron moiety. Even though the electron-transfer sites may to a first-order approximation be viewed as localized on one or another redox center, IR and ESR results reveal some distribution of charge and/or spin to other parts of the cluster. Chart 1 identifies

[†] University of Vermont.
[‡] University of North Texas.
[§] Texas Christian University.

(1) Raithby, P. R. *Platinum Metals Rev.* **1998**, *42*, 146.
(2) Adams, R. D.; Barnard, T. S. *Organometallics* **1998**, *17*, 2885.
(3) (a) Mukerjee, S.; Srinivasan, S.; Soriaga, M. P.; McBreen, J. *J. Electrochem. Soc.* **1995**, *142*, 1409 (b) McBreen, J.; Mukerjee, S. *J. Electrochem. Soc.* **1995**, *142*, 3399.
(4) Zhou, M.; Pfennig, B. W.; Steiger, J.; Van Engen, D.; Bocarsly, A. B. *Inorg. Chem.* **1990**, *29*, 2456.
(5) Averill, B. A. *Struct. Bonding* (*Berlin*) **1983**, *53*, 59.
(6) Al-Ahmad, S. A.; Salifoglou, A.; Kanatzidis, M. G.; Dunham, W. R.; Coucouvanis, D. *Inorg. Chem.* **1990**, *29*, 927.
(7) Kostic, N. M. In *Metal Ions in Biological Systems*; Sigel, H., Sigel, A., Eds.; Marcel Dekker: New York, Vol. 27, 1991; p 129 ff.
(8) Sidebotham, R. P.; Beer, P. D.; Hamon, T. A.; Jones, C. J.; McCleverty, J. A. *J. Organomet. Chem.* **1989**, *371*, C31.
(9) Williams, P. D.; Curtis, M. D. *J. Organomet. Chem.* **1988**, *352*, 169.
(10) Nashner, M. S.; Somerville, D. M.; Lane, P. D.; Adler, D. L.; Shapley, J. R.; Nuzzo, R. G. *J. Am. Chem. Soc.* **1996**, *118*, 12964.
(11) (a) Zanello, P. *Coord. Chem. Rev.* **1988**, *87*, 1. (b) Lemoine, P. *Coord. Chem. Rev.* **1988**, *83*, 169.

10.1021/om010838a CCC: $22.00
Publication on Web 02/16/2002

Chart 1

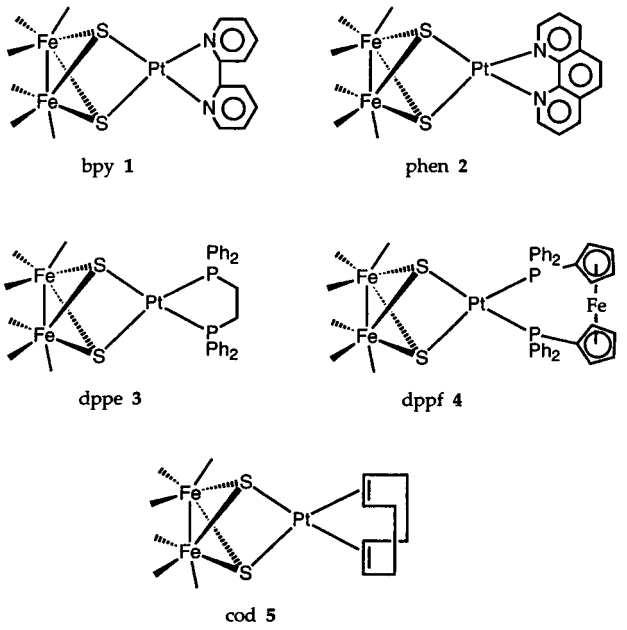

the individual complexes $Fe_2(CO)_6(\mu_3\text{-}S)_2PtL_2$ studied, where L_2 = bipyridine (bpy), **1**, phenanthroline (phen), **2**, diphenylphosphinoethane (dppe), **3**, (bis)diphenylphosphinoferrocene (dppf), **4**, and cyclooctadiene (cod), **5**.

Experimental Section

All operations were performed under an atmosphere of inert gas using standard Schlenk or controlled-atmosphere techniques[12] in dried and distilled solvents. Synthetic procedures were generally carried out under argon, whereas electrochemical work was under nitrogen. Combustion analyses were performed by Atlantic Microlab, Norcross, GA.

Reagents. The tricobalt cluster $Co_3(CO)_9(\mu_3\text{-}CCH_3)$ was prepared according to the literature,[13] as were $Fe_2(CO)_6(\mu_2\text{-}S_2)$[14] and the platinum dichlorides $PtCl_2$(cod), $PtCl_2$(phen), $PtCl_2$(bpy), $PtCl_2$(dppe), and $PtCl_2$(dppf).[15]Ferrocene and decamethylferrocene were obtained commercially (Strem Chemicals) and used as received, as was Super Hydride (1.0 M in THF) and $Fe(CO)_5$ (Aldrich Chemical Co.). $[NBu_4][PF_6]$ was prepared by metathesis of $[NBu_4]I$ and $[NH_4][PF_6]$ and recrystallized several times from 95% ethanol before being vacuum-dried for 2 days at 373 K. $[NBu_4][CF_3SO_3]$ was prepared by the method of Rousseau and co-workers[16] and recrystallized three times from 1:1 dichloromethane/diethyl ether before undergoing a similar drying procedure. The one-electron oxidant $[(p\text{-}BrC_6H_4)_3N][BF_4]$ was prepared by a procedure similar to that described for the $[SbCl_6]$ salt.[17]

$Fe_2(CO)_6(\mu_3\text{-}S)_2PtL_2$. Since the syntheses of the various $Fe_2(CO)_6(\mu_3\text{-}S)_2PtL_2$ complexes employed identical procedures, only the specific reaction conditions for the complex with L_2 = bpy will be described in detail. IR spectra were obtained on CH_2Cl_2 solutions, and absorptions in the carbonyl region are listed in Table 4. NMR spectra were obtained in $CDCl_3$. To the dianion of $Fe_2(CO)_6(\mu_2\text{-}S)_2$, prepared from 0.20 g (0.58 mmol) of $Fe_2(CO)_6(\mu_2\text{-}S)_2$ and 1.22 mL of Super Hydride (slight molar excess), in THF at 195 K was added 0.25 g (0.58 mmol) of $PtCl_2$(bpy) against a counterflow of argon. The reaction was stirred for 2.0 h at this temperature, followed by warming to room temperature. Since IR and TLC analyses revealed that the reaction had gone to completion, the solvent was removed under vacuum to afford a red solid. The product was subsequently chromatographed on silica gel using dichloromethane as the eluant.

Recrystallization of the cluster from CH_2Cl_2 gave red $Fe_2(CO)_6(\mu_3\text{-}S)_2Pt$(bpy) (**1**), yield 0.33 g (82%). Anal. (Calcd) for $C_{16}H_8Fe_2N_2O_6PtS_2$: C, 27.65 (27.49); H, 1.16 (1.22)

$Fe_2(CO)_6(\mu_3\text{-}S)_2Pt$(phen) (2): 84% yield, recrystallized from toluene. Anal. (Calcd) for $C_{18}H_8Fe_2N_2O_6PtS_2\cdot 1/6C_7H_8$: C, 31.03 (31.34); H, 1.24 (1.28).

$Fe_2(CO)_6(\mu_3\text{-}S)_2Pt$(dppe) (3): 94% yield, recrystallized from toluene. $^{31}P\{^1H\}$: δ 39.90 ($J_{Pt,\,P}$ = 2721 Hz). Anal. (Calcd) for $C_{32}H_{24}Fe_2N_2O_6P_2PtS_2\cdot 1/4C_7H_8$: C, 42.21 (42.18); H, 2.73 (2.80).

$Fe_2(CO)_6(\mu_3\text{-}S)_2Pt$(dppf) (4): 88% yield, recrystallized from CH_2Cl_2. $^{31}P\{^1H\}$: δ 19.10 ($J_{Pt,\,p}$ = 2849 Hz). Anal. (Calcd) for $C_{40}H_{28}Fe_2O_6P_2PtS_2\cdot CH_2Cl_2$: C, 41.79 (41.76); H, 2.57 (2.63).

$Fe_2(CO)_6(\mu_3\text{-}S)_2Pt$(cod) (5): 83% yield, recrystallized from CH_2Cl_2. Anal. (Calcd) for $C_{14}H_{12}Fe_2O_6PtS_2$: C, 25.98 (26.03); H, 1.87 (1.91).

Table 1. X-ray Crystallographic Data and Processing Parameters for $Fe_2(CO)_6(\mu_3\text{-}S)_2Pt$(phen) (2) and $Fe_2(CO)_6(\mu_3\text{-}S)_2Pt$(COD) (5)

	2	**5**
space group	$P\bar{1}$, triclinic	$P\bar{1}$, triclinic
a, Å	7.688(1)	7.685(1)
b, Å	11.118(2)	11.363(2)
c, Å	13.257(2)	11.403(2)
α, deg	70.26(1)	113.92(1)
β, deg	76.25(1)	100.57(1)
γ, deg	78.68(1)	90.78(1)
V, Å^3	1027.7(3)	890.5(2)
mol formula	$C_{18}H_8Fe_2N_2O_6PtS_2$	$C_{14}H_{12}Fe_2O_6PtS_2$
fw	719.19	647.15
formula units per cell (Z)	2	2
ρ, g·cm^{-3}	2.324	2.41
abs coeff (μ), cm^{-1}	87.67	101.0
λ(Mo Kα), Å	0.71073	0.71073
collecn range, deg	$3.0 \le 2\theta \le 50.0$	$3.0 \le 2\theta \le 50.0$
tot. no. of data collcd	3623	3145
no. of indep data, $I > 3\sigma(I)$	3257	3017
no. of params	280	227
R	0.0356	0.0484
R_w	0.0381	0.0641
GOF	1.309	1.109
weights	$w = [\sigma^2(F_o) + 2.2 \times 10^{-7}F_o^2]^{-1}$	$w = [\sigma^2(F_o) + 2.2 \times 10^{-7}F_o^2]^{-1}$

Electrochemical Procedures. Electrochemical cells within the drybox were temperature-controlled to better than one degree precision by immersing the cells in a heptane bath controlled by an FTS Systems refrigeration probe. All potentials in this paper are referenced to the ferrocene/ferrocenium couple, although the experimental reference electrode was a Ag/AgCl electrode, made by anodizing silver wire in an HCl solution. The reference electrode was kept separated from the solution containing the test compound by a fine sintered frit. The ferrocene potential was obtained by direct addition of Cp_2Fe to the test solution at a suitable point in the experiment. Solid disks were used as the working electrodes for all cyclic voltammetry (CV) scans. Obtained from Bioanalytical Systems, they were polished successively with 6, 3, 1, and then 0.25 μm diamond paste (Metadi II, Buehler) on a polishing cloth, with copious washings with Nanopure water between polishings. The nominal sizes of the electrodes were either 3 mm (glassy C) or 2 mm (Pt and Au). Rotating electrode voltam-

(12) Shriver, D. F.; Drezdzon, M. A. *The Manipulation of Air-Sensitive Compounds*, 2nd ed.; John Wiley and Sons: New York, 1986.
(13) Seyferth, D.; Hallgren, J. E.; Hung, P. L. K. *J. Organomet. Chem.* **1973**, *50*, 265.
(14) Hieber, W.; Gruber, J. *Z. Anorg. Allg. Chem.* **1958**, *296*, 91.
(15) (a) Drew, D.; Doyle, J. R. *Inorg. Synth.* **1973**, *13*, 48. (b) Watt, G. W.; Cuddeback, J. E. *J. Inorg. Nucl. Chem.* **1971**, *33*, 259. (c) Morgan, G. T.; Burstall, F. H. *J. Chem. Soc.* **1934**, 965. (d) Corain, B.; Longato, B.; Favero, G.; Ajo, D.; Pilloni, G.; Russo, U.; Kreissl, F. R. *Inorg. Chim. Acta* **1989**, *157*, 259.
(16) Rousseau, K.; Farrington, G. C.; Dolphin, D. *J. Org. Chem.* **1972**, *37*, 3968.

Table 2. Selected Bond Distances (Å) and Angles (deg) for $Fe_2(CO)_6(\mu_3\text{-}S)_2Pt(phen)$ and $Fe_2(CO)_6(\mu_3\text{-}S)_2Pt(cod)$[a]

$Fe_2(CO)_6(\mu_3\text{-}S)_2Pt(phen)$			
Bond Distances			
Pt−S(1)	2.266(2)	Pt−S(2)	2.258(2)
Pt−N(1)	2.056(6)	Pt−N(10)	2.064(6)
Fe(1)−Fe(2)	2.492(2)	Fe(1)−S(1)	2.292(2)
Fe(1)−S(2)	2.299(2)	Fe(2)−S(2)	2.290(3)
Fe(2)−S(2)	2.281(2)	N(1)−C(2)	1.339(9)
N(1)−C(10b)	1.366(10)	C(2)−C(3)	1.375(14)
C(3)−C(4)	1.341(15)	C(4)−C(4a)	1.408(11)
C(4a)−C(5)	1.434(15)	c(4a)−C(10b)	1.411(13)
C(5)−C(6)	1.330(12)	C(6)−C(6a)	1.445(15)
C(6a)−C(7)	1.407(11)	C(6a)−C(10a)	1.407(12)
C(7)−C(8)	1.364(16)	C(8)−C(9)	1.404(13)
C(9)−N(10)	1.319(9)	N(10)−C(10a)	1.363(11)
C(10a)−C(10b)	1.412(9)		
Bond Angles			
S(1)−Pt−S(2)	77.4(1)	S(1)−Pt−N(1)	101.1(2)
S(2)−Pt−N(1)	176.7(2)	S(1)−Pt−N(10)	176.3(2)
S(2)−Pt−N(10)	101.0(2)	N(1)−Pt−N(10)	80.4(2)
Fe(2)−Fe(1)−S(1)	57.0(1)	Fe(2)−Fe(1)−S(2)	56.7(1)
S(1)−Fe(1)−S(2)	76.0(1)	S(1)−Fe(2)−S(2)	76.4(1)
Pt−S(1)−Fe(1)	90.3(1)	Pt−S(1)−Fe(2)	95.8(1)
Fe(1)−S(1)−Fe(2)	65.9(1)	Pt−S(2)−Fe(1)	90.3(1)
Pt−S(2)−Fe(2)	96.2(1)	Fe(1)−S(2)−Fe(2)	65.9(1)
$Fe_2(CO)_6(\mu_3\text{-}S)_2Pt(cod)$			
Bond Distances			
Pt−S(1)	2.288(2)	Pt−S(2)	2.287(2)
Pt−C(1)	2.219(7)	Pt−C(2)	2.191(7)
Pt−C(5)	2.223(11)	Pt−C(6)	2.196(10)
Fe(1)−Fe(2)	2.501(2)	Fe(1)−S(1)	2.276(3)
Fe(1)−S(2)	2.272(2)	Fe(2)−S(1)	2.284(3)
Fe(2)−S(2)	2.279(2)	C(1)−C(2)	1.368(14)
C(5)−C(6)	1.348(14)		
Bond Angles			
S(1)−Pt−S(2)	77.9(1)	S(1)−Pt−C(1)	166.2(3)
S(2)−Pt−C(1)	98.7(3)	S(1)−PT−C(2)	156.7(2)
S(2)−Pt−C(2)	96.1(3)	C(1)−Pt−C(2)	36.1(4)
S(1)−Pt−C(5)	98.4(2)	S(2)−Pt−C(5)	164.8(2)
C(1)−Pt−C(5)	88.2(3)	C(2)−Pt−C(5)	81.5(3)
S(1)−Pt−C(6)	96.9(2)	S(2)−Pt−C(6)	158.8(3)
C(1)−Pt−C(6)	81.4(3)	C(2)−Pt−C(6)	96.1(3)
C(5)−Pt−C(6)	35.5(4)	Fe(2)−Fe(1)−S(1)	56.9(1)
Fe(2)−Fe(1)−S(2)	56.8(1)	S(1)−Fe(1)−S(2)	78.5(1)
Fe(1)−Fe(2)−S(1)	56.6(1)	Fe(1)−Fe(2)−S(2)	56.5(1)
S(1)−Fe(2)−S(2)	78.2(1)	Pt−S(1)−Fe(1)	93.2(1)
Pt−S(1)−Fe(2)	89.8(1)	Fe(1)−S(1)−Fe(2)	66.5(1)
Pt−S(2)−Fe(1)	93.3(1)	Pt−S(2)−Fe(2)	90.0(1)
Fe(1)−S(2)−Fe(2)	66.7(1)		

[a] Numbers in parentheses are estimated standard deviations in the least significant digits.

metry was most reproducible when a film of mercury had been deposited on the Pt electrode rotated at 1800 rpm. The mercury deposition procedure has been described.[18] Controlled potential coulometry was performed in a cell in which the anodic and cathodic compartments were separated by a 20 mm fine frit. When THF was used in these experiments, a few milligrams of ferrocene added to the auxiliary electrode compartment largely eliminated problems arising from anodic polymerization of the solvent. A Pt gauze basket was used as the working electrode in bulk electrolyses. Electrochemical instrumentation was as previously described.[19] The response of each electrode reaction was subjected to diagnostics for diffusion control and chemical and electrochemical reversibility, using criteria previously summarized.[20]

Table 3. Electrochemical Potentials of Clusters $Fe_2(CO)_6(\mu_3\text{-}S_2)PtL_2$ in Volts vs Ferrocene

			reductions		oxidations	
complex	L_2	solvent	0/1−[a]	1−/3−	0/1+[a]	1+/2+[b]
1	bpy	THF	−1.78	−2.32[c]		
		CH_2Cl_2			0.19	0.56
2	phen	THF	−1.79	−2.3[c]		
		CH_2Cl_2			0.20	0.57
			0/2-		0/1+	1+/2+
3	dppe	THF	−2.17[c]			
		CH_2Cl_2			0.13	0.69
4	dppf	THF	−2.36[d]			
		CH_2Cl_2			0.16	0.76[a]
5	cod	THF	−1.95[d]			
		CH_2Cl_2			0.38	0.69

[a] Chemically reversible couple at ambient temperatures, $E_{1/2}$ given. [b] Irreversible at temperatures down to 233 K, E_{pc} given. [c] Fully chemically reversible at 233 K, $E_{1/2}$ at this temperature given. [d] Irreversible down to 218 K, E_{pc} given.

Table 4. Carbonyl IR Frequencies (in cm^{-1}) for the Clusters $Fe_2(CO)_6(\mu_3\text{-}S_2)PtL_2$ and Their Oxidation and Reduction Products

	parent compound				
charge on compound	**1**	**2**	**3**	**4**	**5**
0	2049	2049	2046	2047	2057
	2009	2009	2006	2007	2057
	1968[a]	1968[a]	1967	1969	1979
	1964[a]	1964[a]	1960	1959	1976
1−	2037	2037			
	1996	1996			
	1950	1951			
2−			1946		
			1899		
			1860		
3−	1931				
	1892				
	1852				
unassigned anion					2023
					2000
					1943
1+	2117	2108	2092	2118	2126
	2095	2090	2055	2103	2102
	2062	2051	2034	2073	2066
	2035	2030	2025	2036	2042
				2026	

Spectroscopy. IR spectra were obtained using sealed NaCl cells of 0.48 mm path length (Spectra-Tech) in a Mattson Polaris FTIR spectrometer operating at 2 cm^{-1} resolution. Spectra of electrolysis products were obtained by transferring within the drybox about 0.2 mL of an electrolysis solution to the IR cell using a glass syringe, after both the cell and the syringe had been precooled with cold nitrogen. The cell was immediately removed from the drybox and put into a cold sample holder in the IR sample chamber. This procedure frequently resulted in a minor amount of regeneration of a neutral cluster in solutions containing the cluster monoanions, but spectra of the latter were readily obtained by spectral subtraction of a certain amount of the IR spectrum of the neutral complexes (see Figure 6, for example). ESR sampling proceeded by a similar procedure, the transferred samples being immediately frozen in liquid nitrogen and kept at 77 K until spectra were recorded. A modified Varian E-4 spectrometer was used for ESR measurements using dpph (Aldrich) as a *g*-value standard. ESR simulations were performed using a program developed by L. K. White and R. L. Belford and

(17) (a) Schmidt, W.; Steckhan, E. *Chem. Ber.* **1980**, *113*, 577. (b) Dapperheld, S.; Steckhan, E.; Grosse Brinkhaus, K.-H.; Esch, T. *Chem. Ber.* **1991**, *124*, 2557.
(18) Ramaley, L.; Brubaker, R. L.; Enke, C. G. *Anal. Chem.* **1963**, *35*, 1088.
(19) Orsini, J.; Geiger, W. E. *Organometallics* **1999**, *18*, 1854.
(20) Geiger, W. E. In *Laboratory Techniques in Electro-analytical Chemistry*, 2nd ed.; Kissinger, P. T., Heineman, W. R., Eds.; Marcel Dekker: New York, 1996; Chapter 23.

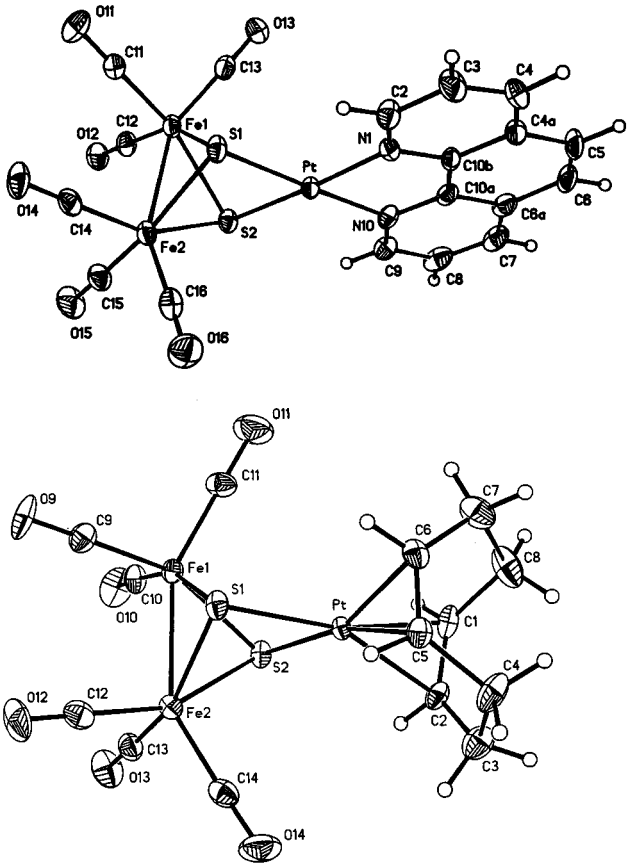

Figure 1. ORTEP diagrams of $Fe_2(CO)_6(\mu_3\text{-}S)_2Pt(phen)$ (top) and $Fe_2(CO)_6(\mu_3\text{-}S)_2Pt(cod)$ (bottom) showing the thermal ellipsoids at the 35% and 30% probability levels, respectively.

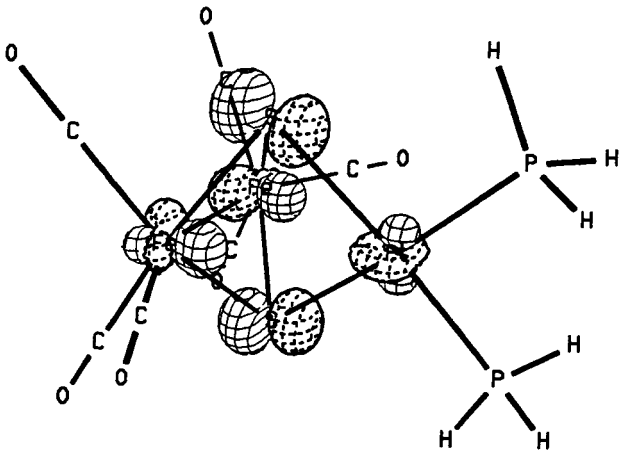

Figure 2. CACAO drawing of the HOMO for $Fe_2(CO)_6(\mu_3\text{-}S)_2Pt(PH_3)_2$.

subsequently modified by White, N. F. Albanese, and N. D. Chasteen. We thank Prof. Chasteen (University of New Hampshire) for a copy of the program. ^{31}P NMR data were recorded at 121 MHz on a Varian 300-VXR spectrometer.

X-ray Diffraction Data. Single crystals of $Fe_2(CO)_6(\mu_3\text{-}S)_2Pt(phen)$, **2**, were grown from CH_2Cl_2. A suitable crystal having dimensions of 0.05 × 0.15 × 0.38 mm^2 was selected and mounted on a Nicolet R3M/μ update of a P1 diffractometer. Cell constants were obtained from a least-squares refinement of 25 reflections in the range 25.05° ≤ 2θ ≤ 29.08°. Laue symmetry and statistics were consistent with the $P2_1$ space group. Intensity data in the range 3.0° ≤ 2θ ≤ 50.0° were collected at 295 K in the ω-scan mode using a variable-scan speed and graphite-monochromated Mo Kα radiation (λ = 0.71073). The angles were measured by a centering routine. Lorentz−polarization corrections and a Ψ-scan-based empirical absorption correction were applied (transmission factors 1.000−0.417). The structure was solved by direct methods and refined by a block-cascade least-squares technique. All hydrogens were located in the difference map and refined with isotropic thermal parameters. All non-hydrogen atoms were refined anisotropically. Refinement converged to $R = 0.0356$ and $R_w = 0.0381$ for 3257 unique reflections with $I > 3\sigma(I)$.

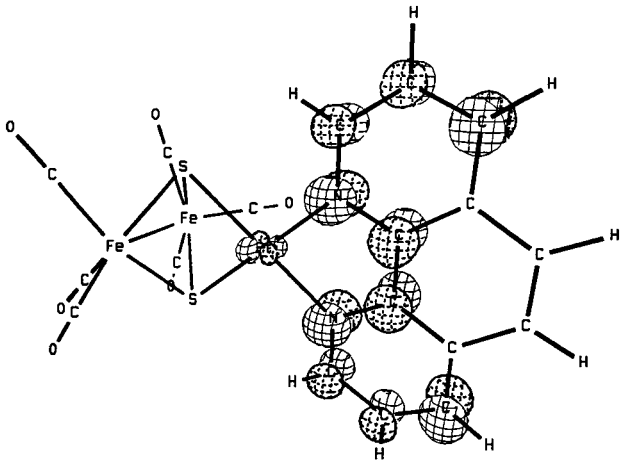

Figure 3. CACAO drawing of the LUMO for $Fe_2(CO)_6(\mu_3\text{-}S)_2Pt(phen)$.

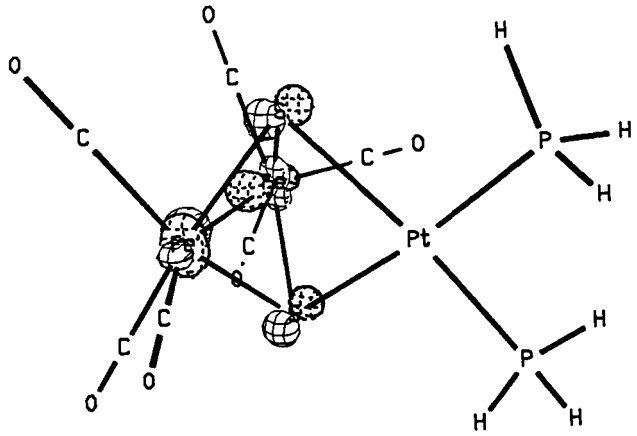

Figure 4. CACAO drawing of the LUMO for $Fe_2(CO)_6(\mu_3\text{-}S)_2Pt(PH_3)_2$.

The structure of $Fe_2(CO)_6(\mu_3\text{-}S)_2Pt(cod)$ (**5**) was determined in an analogous fashion. The structure was solved by direct methods and refined by a block-cascade least-squares technique. All hydrogen atoms were located in the difference map and refined with isotropic parameters. All non-hydrogen atoms were refined anisotropically. Refinement converged to $R = 0.0484$ and $R_w = 0.0641$ for 3017 unique reflections with $I > 3\sigma(I)$.

Extended Hückel MO Calculations. The EHMO calculations on the clusters $Fe_2(CO)_6(\mu_3\text{-}S)_2Pt(phen)$, $Fe_2(CO)_6(\mu_3\text{-}S)_2Pt(PH_3)_2$, and $Fe_2(CO)_6(\mu_3\text{-}S)_2Pt(ethylene)_2$ were carried out with the program originally developed by Hoffmann[21] and modified by Mealli and Proserpio.[22] The input *Z*-matrix for these clusters, confined to idealized C_{2v} symmetry, was prepared by using the bond distances and bond angles from the X-ray data on $Fe_2(CO)_6(\mu_3\text{-}S)_2Pt(phen)$, $Fe_2(CO)_6(\mu_3\text{-}S)_2Pt(cod)$ and related structurally characterized Fe_2S_2Pt clusters.

(21) (a) Hoffmann, R.; Lipscomb, W. N. *J. Chem. Phys.* **1962**, *36*, 3179. (b) Hoffmann, R. *J. Phys. Chem.* **1963**, *39*, 1397.
(22) Mealli, C.; Proserpio, D. M. *J. Chem. Educ.* **1990**, *67*, 399.

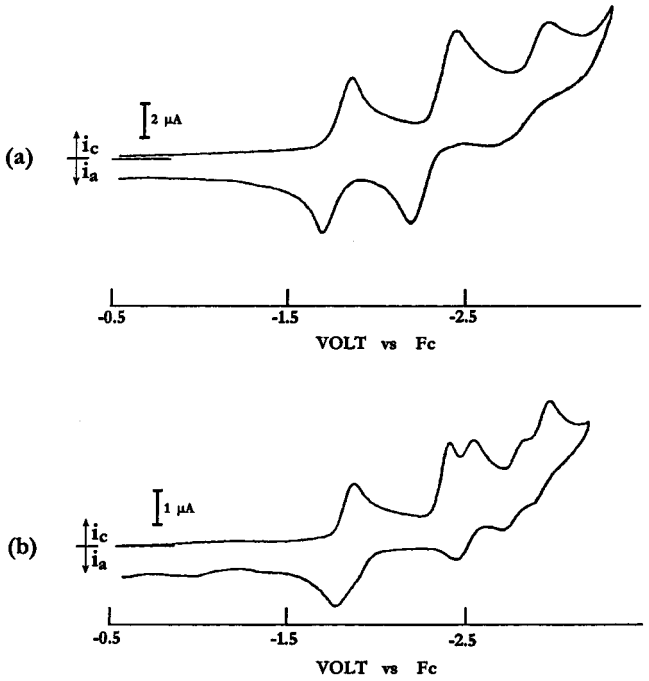

Figure 5. Cyclic voltammograms of reductions of **1** in THF/0.1 M $[NBu_4][X]$ at a Pt electrode. (a) 0.30 mM **1**, X = CF_3SO_3, T = 233 K, ν = 0.5 V/s; (b) 0.53 mM **1**, X = PF_6, room temperature, ν = 0.2 V/s.

Results and Discussion

Structure of Clusters and LUMO/HOMO Identities. Figure 1 shows the ORTEP diagram for the phenanthroline and cyclooctadiene clusters **2** and **5**, respectively. The X-ray data and processing parameters are listed in Table 1, and selected bond distances and angles are given in Table 2.

The basic cluster cores of these two complexes are similar in that they both exhibit an Fe_2S_2Pt framework. The *arachno* five-vertex polyhedral shape for **2** and **5** is theoretically supported through the application of PSEP theory.[23] The Fe−Fe, Fe−S, and S−Pt distances all fall within the range of acceptable values for analogous bonds in related compounds.[24] The coordination of the ancillary phen or cod ligand to Pt shows no unusual structural features relative to other square-planar Pt mononuclear complexes.[25] The remaining distances and angles are unexceptional and require no discussion.

The EHMO studies indicate that the HOMOs of compounds **1**−**5** are virtually identical but that the LUMOs of **1** and **2** differ from those of **3**−**5**.

Considering first the HOMO, the cluster **2** was calculated directly; $Fe_2(CO)_6(\mu_3\text{-}S)_2Pt(PH_3)_2$ was calculated as a model for **3** and **4**, and $Fe_2(CO)_6(\mu_3\text{-}S)_2Pt(ethylene)_2$ was used to model **5**. The orbital composition

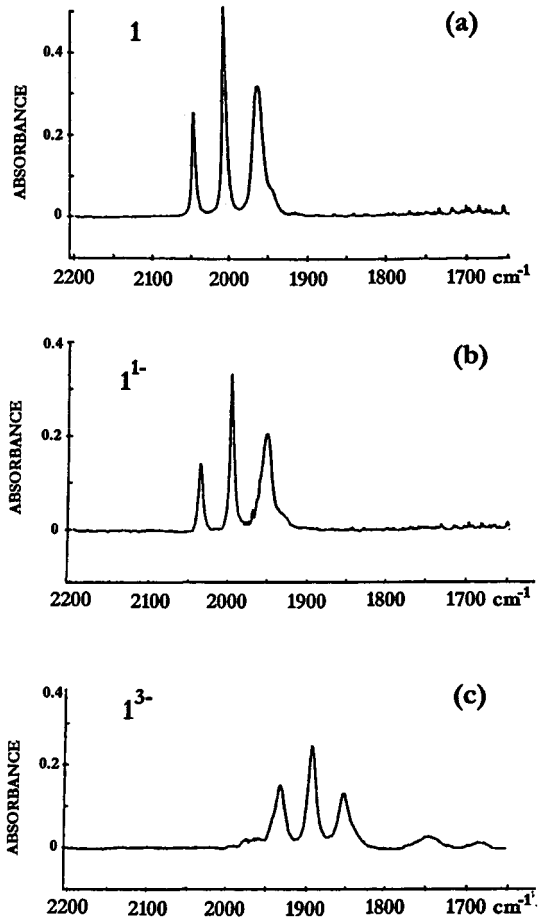

Figure 6. IR spectra of neutral **1** (a), monoanion $\mathbf{1}^-$ (b), and the probable trianion $\mathbf{1}^{3-}$ (c). Spectra were recorded after bulk electrolytic reductions of 1 mM **1** in THF/0.1 M $[NBu_4][CF_3SO_3]$ at E_{appl} = −2.1 V (b) or −2.6 V (c) and are shown after subtraction of features of 0.24 equiv of neutral **1** in (b) or 0.32 equiv of $\mathbf{1}^-$ in (c).

of all three systems is virtually identical; the HOMO at ca. −10.80 eV is best described as a bonding orbital localized almost entirely (88−91%) on the $Fe_2(\mu_3\text{-}S)_2$ moiety, with the Pt center accounting for the remaining contribution. The CACAO drawing[22] of the HOMO (Figure 2) for $Fe_2(CO)_6(\mu_3\text{-}S)_2Pt(PH_3)_2$ shows the overall bonding interaction involving the $Fe_2(\mu_3\text{-}S)_2Pt$ polyhedral core. The hybridized d_{yz} Fe centers are readily discerned and show an in-phase overlap with the bridging sulfido-p_z orbitals. The Pt center is tethered to the $Fe_2(\mu_3\text{-}S)_2$ fragment through the $d_{x^2-y^2}$ orbital that contains added 6s and $6p_z$ character. The theoretical conclusion that the Pt center makes only a minor contribution to the HOMO is well-substantiated by the experimental data discussed below.

Two different types of LUMOs are found in this series of clusters. For **2** the LUMO was found to reside on the Pt(phen) portion of the molecule. The CACAO drawing of the LUMO (Figure 3), which occurs at −9.61 eV and exhibits b_2 symmetry, clearly shows that it is best described as a ligand-based orbital involving the π^* system of the phenanthroline ligand (95%). The Pt orbital contribution to the LUMO amounts to about 4% and derives from the d_{yz} orbital that has been hybridized with the metal p_y orbital.[26] The hybridized platinum orbital has the correct symmetry and nodal character

(23) (a) Wade, K. *Adv. Inorg. Chem. Radiochem.* **1976**, *21*, 146. (b) Mingos, D. M. P.; Wales, D. J. *Introduction to Cluster Chemistry*; Prentice-Hall: New York, 1990.

(24) (a) Don, M.-J.; Yang, K.; Bott, S. G.; Richmond, M. G. *J. Coord. Chem.* **1996**, *40*, 273. (b) Cowie, M.; DeKock, R. L.; Wagenmaker, T. R.; Seyferth, D.; Henderson, R. S.; Gallagher, M. K. *Organometallics* **1989**, *8*, 119. (c) Bose, K. S.; Sinn, E.; Averill, B. A. *Organometallics* **1984**, *3*, 1126. (d) Song, L.-C.; Kadiata, M.; Wang, J.-T.; Wang, R.-J.; Wang, H.-G. *J. Organomet. Chem.* **1990**, *391*, 387. (e) Adams, R. D.; Huang, M.; Wu, W. *J. Cluster Sci.* **1997**, *8*, 115.

(25) (a) Keefer, C. E.; Bereman, R. D.; Purrington, S. T.; Knight, B. W.; Boyle, P. D. *Inorg. Chem.* **1999**, *38*, 2294. (b) Bevilacqua, J. M.; Zuleta, J. A.; Eisenberg, R. *Inorg. Chem.* **1993**, *32*, 3689.

so as to minimize the antibonding Pt-π* phen interaction inherent in the LUMO. The bipyridine complex **1** is expected to have virtually identical bonding.

Compared to the result for **2**, the determination of the LUMO in $Fe_2(CO)_6(\mu_3\text{-}S)_2Pt(PH_3)_2$ and $Fe_2(CO)_6(\mu_3\text{-}S)_2Pt(ethylene)_2$ was not as clear. Calculations on the two latter complexes revealed the presence of several close-lying levels, making the LUMO assignment less definitive.

In the case of the PH_3 complex, an antibonding orbital localized almost entirely on the $Fe_2(CO)_6(\mu_3\text{-}S)_2$ fragment was found at −9.09 eV.[27] The LUMO in Figure 4 shows the antibonding interactions within the $Fe_2(\mu_3\text{-}S)_2$ group, whose parentage derives from the overlap of the $d_{x^2-y^2}$ (Fe) and p_y (S) orbitals. Not shown in the CACAO drawing is the considerable π* contributions from the ancillary CO groups. The observation (vide infra) of a two-electron reduction for compounds **3**−**5** is certainly consistent with a LUMO possessing Fe−Fe antibonding character.

Electrochemistry. Overview of Electron-Transfer Processes. Electron-transfer reactions involving sequential transfer of as many as five electrons are observed for the 50-electron clusters $Fe_2(CO)_6S_2PtL_2$. Chemically reversible reductive processes gave polyanions containing as many as 53 e^- and anodic processes gave in each case a stable 49 e^- species; further oxidations to 48 e^- dications were generally irreversible. Details of the voltammetric and electrolytic diagnostics used to reach these conclusions are given in the Experimental Section; in general, a variety of temperatures, solvents, and scan rates were used to investigate each redox process. The potentials of the various electrode reactions are collected in Table 3.

Reductions. Each complex undergoes a single-step two-electron reduction which, in the cases of **1** and **2**, is preceded by a separate one-electron reduction. As will be shown below and as suggested by the EHMO calculations, the one-electron processes for **1** and **2** are localized on the PtL_2 part of the complex (L_2 = bpy or phen); the two-electron processes appear to involve the Fe_2S_2 moiety.

1 and 2: Formation of Mono- and Trianions. Complexes **1** and **2** display two chemically reversible reductions at subambient temperatures (Figure 5a) in addition to an irreversible third wave at more negative potentials, which was not investigated in detail. The first of these was also reversible at room temperature and fits all the diagnostics of a reversible one-electron process giving a stable monoanion, e.g., $\mathbf{1}^-$. Included in the diagnostics is the fact that the cathodic current of **1** was essentially the same as that of the known[28] one-electron process for the cluster $Co_3(CO)_9(\mu\text{-}CMe)$, which was chosen as a "standard" owing to its expected similar diffusion coefficient [the current function,[20] $i_{pc}/\nu^{1/2}$, of **1** relative to equimolar $Co_3(CO)_9(\mu\text{-}CMe)$ was 1.05; plateau current at rotating Pt electrode (rpe), 0.94]. A bulk electrolysis of **1** in THF/0.1 M $[NBu_4][CF_3SO_3]$ at E_{appl} = −2.1 V, T = 228 K, resulted in a color change from light red to dark red and essentially quantitative formation of $\mathbf{1}^-$, as judged by the limiting currents in rpe voltammograms. Passage of 1.0 F/eq confirmed the one-electron stoichiometry of the reaction. Samples of the monoanion were withdrawn for IR and ESR analysis (vide infra). Back-oxidation with E_{appl} = −0.9 V resulted in 90% recovery of the starting material.

The second reduction is 1.6−1.7 times larger than the first when comparing either cathodic current functions or rpe currents. CV peak separations were increased over those observed for Nernstian standards (e.g., ΔE_p = 135 mV at ν = 0.1 V/s at 233 K, compared to 95 mV for decamethylferrocene and 94 mV for $\mathbf{1}/\mathbf{1}^-$). The chemical reversibility of the second wave was confirmed by scan−hold−scan experiments,[29] which showed $i_{reverse}/i_{fwd} = 1.02 \pm 0.03$ at scan rates between 0.1 and 0.5 V/s. This wave has the characteristics of a chemically reversible two-electron process having quasi-reversible charge-transfer kinetics. The primary reductive processes of **1** (and **2**) can therefore be represented in eq 1:

$$\mathbf{1} \overset{e^-}{\rightleftharpoons} \mathbf{1}^- \overset{2e^-}{\rightleftharpoons} \mathbf{1}^{3-} \qquad (1)$$

Definitive confirmation of the electron stoichiometry of the second reduction could not be achieved by coulometry, for reasons that are apparent from CV scans taken at room temperature (Figure 5b). The trianion of **1** is not completely stable at higher temperatures on the CV time scale, nor at 233 K over the electrolysis time scale. An applied electrolysis potential sufficient to reach the second reduction process is sufficient to electrolyze the product of decomposition of the trianion. Consistent with this, about 4 F/eq were consumed for electrolysis of **1** with E_{appl} = −2.6 V, rather than the 3 F/eq expected from eq 1. Even at T = 208 K, some decomposition waves were observed after an electrolysis, including one with $E_{1/2}$ = −2.74 V, which matches the potential for the reduction of free bpy.

IR spectra of electrolysis solutions taken at the monoanionic stage displayed a three-band pattern in the CO region for $\mathbf{1}^-$ (Figure 6b) that is consistent with an intact $Fe_2(CO)_6$ moiety, but the energies (Table 4) are shifted lower (Table 5) by only about 14 cm^{-1} compared to **1**. This indicates that *the LUMO of **1** does not have significant iron character*. ESR spectra of $\mathbf{1}^-$ confirm this (vide infra).

IR spectra of solutions electrolyzed at the second reduction wave at 208 K were able to detect two CO-containing species (Figure 6c): roughly a 30% yield of $\mathbf{1}^-$ and a 50% yield of a species having a three-band

(26) The apparent discrepancy between the ESR designation of the LUMO as a $(\pi^*)^1(d_{xy})^0$ state and the MO description of this orbital as a $(\pi^*)^1(d_{yz})^0$ state derives from the method in which the CACAO program sets up the *Z*-matrix. Here the calculations are carried out with the main symmetry axis conincident with the *z*-axis.

(27) The two likely LUMO candidates are separated by about 0.14 and 0.54 eV, respectively, in the PH_3 and ethylene clusters. Moreover, the results are extremely sensitive to the positioning of the Pt center relative to the Fe−Fe bond, leading to an orbital crossing of the antibonding $Fe_2(\mu_3\text{-}S)_2$-based orbital with a platinum-based orbital that displays antibonding Pt−S and Pt−L character.

(28) (a) Kotz, J. C.; Petersen, J. V.; Reed, R. C. *J. Organomet. Chem.* **1976**, *120*, 433. (b) Bond, A. M.; Peake, B. M.; Robinson, B. H.; Simpson, J.; Watson, D. J. *Inorg. Chem.* **1977**, *16*, 410. (c) Bond, A. M.; Dawson, P. A.; Peake, B. M.; Rieger, P. H.; Robinson, B. H.; Simpson, J. *Inorg. Chem.* **1979**, *18*, 1413.

(29) In a scan−hold−scan experiment the CV scan is interrupted after the forward-going half of the triangular waveform (the negative-going potential direction in the case of a reduction). After at least 30 s, the reverse scan is initiated. In this way a steady-state concentration of the cathodic electrolysis product ($\mathbf{1}^{3-}$ in our case) is created at the electrode in the "hold" part of the experiment and the anodic-to-cathodic current ratios are measured directly from the peak currents referenced to the zero current line. See: Mabbott, G. A. *J. Chem. Educ.* **1983**, *60*, 697.

Table 5. Shifts of IR Carbonyl Average Energies (in cm^{-1}) for $Fe_2(CO)_6(\mu_3\text{-}S_2)$ PtL_2 Clusters Undergoing Electron Transfer, Referenced to Neutral Complex[a]

	compound				
charge on compound	**1**	**2**	**3**	**4**	**5**
1−	−14	−13			
2−			−104		
3−	−116				
1+	69	62	46	76	67

[a] Computed from the average energy of ν_{CO} bands assigned to compounds and ions (see Table 4).

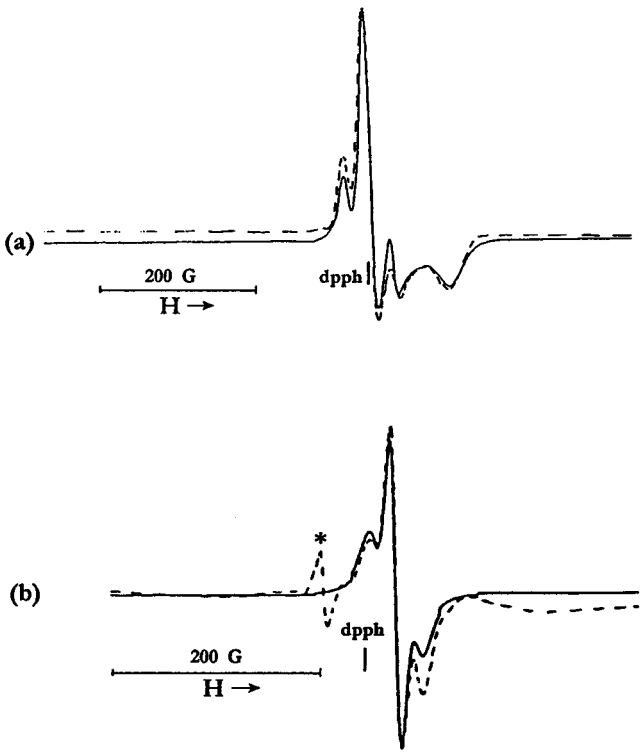

Figure 7. ESR spectra (experimental is dashed line, simulated is solid line) of $\mathbf{1}^-$ obtained after electrolysis (at 218 K) of 1.0 mM **1** in THF/$[NBu_4][CF_3SO_3]$ at E_{appl} = −2.09 V: (a) frozen spectrum (T = 77 K); (b) fluid spectrum at T = 223 K. The resonance position of the external standard dpph is indicated; an asterisk marks the absorption of an apparent decomposition product.

pattern shifted about −115 cm^{-1} from that of **1**, which we tentatively assign to $\mathbf{1}^{3-}$ (because the trianion is subject to some decomposition, we cannot eliminate the possibility that this group of absorptions may arise from an $Fe_2(CO)_6$-containing decomposition product). The additional shift of ≈100 cm^{-1} from the CO absorptions of $\mathbf{1}^-$ is consistent with addition of two additional electrons to a dinuclear $M_2(CO)_x$ center.[30]

ESR spectra of $\mathbf{1}^-$ were recorded for both fluid solutions and those frozen at 77 K. Pt hyperfine splittings (hfs) were noted, and the spectra were simulated (Figure 7a) to give the values in Table 6. Whereas the frozen solution spectra were clean, the presence of a small secondary signal with $\langle g \rangle$ = 2.028 was noted in ambient temperature spectra (Figure 7b). The spectra of $\mathbf{1}^-$ and $\mathbf{2}^-$ are characterized by axial g- and A_{Pt}-tensors. Although some g-value anisotropy is observed ($g_{\|} - g_{\perp}$ ca. 0.06−0.08) and Pt hyperfine splittings of 37 × 10^{-4} and 55 × 10^{-4} cm^{-1} are seen for $\langle a \rangle_{Pt}$ and $A_{\perp}$(Pt), respectively, the degree of metal involvement in the SOMO can be shown to be quite small. The Pt nucleus displays very large splittings in response to admixture of orbital 6s character into the metal d orbital, and a splitting about 1 order of magnitude higher would be expected if the unpaired electron were localized on the Pt atom.[31]Although no ligand hyperfine splittings are observed from, for example, the N atoms in the diimine ligand, this is probably a result of their being unresolved because of the relatively large ESR line widths.

Mixing of the electronic ground state of the monoanion with an empty higher lying orbital is necessary to account for the lack of g-values above 2.0. The ESR data are therefore consistent with an electronic ground state for $\mathbf{1}^-$ and $\mathbf{2}^-$ of the type $(\pi^*)^1(d_{xy})^0$, where the π^* orbital is located on the unsaturated heterocyclic ligand (bpy or phen) and the d_{xy} orbital which mixes in the excited state is located at the square-planar Pt(II) site.

A similar conclusion was reached for anion radicals of the type $[Pt(bpy)L_2]^-$, L = Cl^-, CN^-, mesitylene, on the basis of Pt hyperfine splittings of (40−55) × 10^{-4} cm^{-1} [32,33] and for L = Ph^- on the basis of a Pt hyperfine splitting of less than about 25 × 10^{-4} cm^{-1}.[34]

The combined electrochemistry, IR, and ESR data argue, therefore, for initial reduction at the bpy or phen ligand in **1** and **2**, followed by two-electron reduction involving the $Fe_2(\mu_3\text{-}S)_2$ group.

Complexes 3−5: Single Two-Electron Reductions. This set of molecules is expected to lack the one-electron process in the −1.7 V range owing to the lack of a ligand π^* reduction site. Indeed, the first reduction process of all three complexes occurs in a wave of two-electron height in the −2.0 to −2.4 V range (Table 3). The behavior of this wave was electrode dependent, the most reproducible results being obtained on either Hg or glassy carbon. Figure 8a shows a CV scan of **3** at 238 K. Peak separations were much higher, typically 175 mV at ν = 0.2 V/s, than expected for a Nernstian two-electron wave, so that the reductions must be characterized as quasi-reversible two-electron reactions, eq 2:

$$Fe_2(CO)_6S_2PtL_2 + 2e^- \rightleftharpoons [Fe_2(CO)_6S_2PtL_2]^{2-} \qquad L_2 = \text{dppe, dppf, cod} \quad (2)$$

Like the products of the two-electron waves of **1** and **2** (trianions in those cases), the dianions were stable only at severely reduced temperatures. Figure 8c shows the result of a bulk electrolysis of **3** at 238 K in THF/0.1 M $[NBu_4][CF_3SO_3]$ with E_{appl} = −2.5 V. Exactly 2.0 F/eq were consumed as the solution went from yellow to dark red. The rpe scan after electrolysis showed that the dianion was the dominant reduction product; a reoxidation of the dianion (1.4 F/eq released, Figure 8d) recovered the starting material in 60% yield. IR spectra

(30) For leading references to redox-induced IR shifts for polynuclear complexes see: Robben, M. P.; Rieger, P. H.; Geiger, W. E. *J. Am. Chem. Soc.* **1999**, *121*, 367

(31) Morton, J. R.; Preston, K. F. *J. Magn. Reson.* **1978**, *30*, 577.
(32) Collison, D.; Mabbs, F. E.; McInnes, E. J. L.; Taylor, K. J.; Welch, A. J.; Yellowlees, L. J. *J. Chem. Soc., Dalton Trans.* **1996**, 329.
(33) Klein, A.; Kaim, W. *Organometallics* **1995**, *14*, 1176.
(34) Braterman, P. S.; Song, J.-I.; Vogler, C.; Kaim, W. *Inorg. Chem.* **1992**, *31*, 222.

Table 6. ESR Results for Reduced and Oxidized Clusters: Anions Measured in THF, Cations Measured in 1:1 CH_2Cl_2:$C_2H_4Cl_2$

radical	T (K)	g_1	g_2	g_3	$\langle g \rangle$	$A_{1(Pt)}$[a]	$A_{2(Pt)}$[a]	$A_{3(Pt)}$[a]	$\langle a \rangle_{Pt}$[a]
$\mathbf{1}^-$	77	2.003[b]	2.003[b]	1.940[c]		55[b]	55[b]	<25[c]	
	223				1.984				37
$\mathbf{2}^-$	77	2.003[b]	2.003[b]	1.923[c]		55[b]	55[b]	<25[c]	
	223				1.976				37
$\mathbf{1}^+$	77	2.033	2.004	1.980		202	226	226	
	223				2.007				243
$\mathbf{2}^+$	77	2.033	2.002	1.979		225	235	244	
	223				2.009				252
$\mathbf{3}^+$	77	2.055	2.002	1.973		110	142	126	
$\mathbf{4}^+$	77	2.058	2.003	1.986		135	160	150	
	228				2.015				174
$\mathbf{5}^+$	223				2.025				245

[a] Pt hyperfine splitting in units of 10^{-4} cm^{-1}. [b] Parallel contribution. [c] Perpendicular contribution.

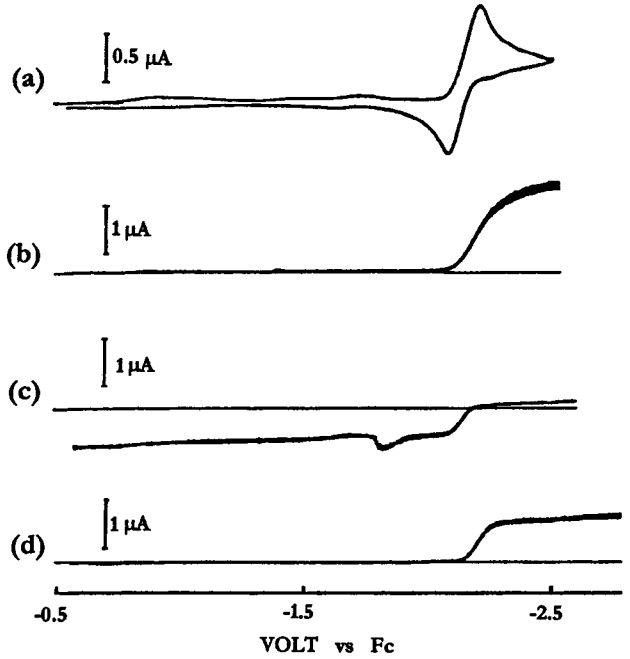

Figure 8. Scans at various points in bulk electrolyses involving 1.1 mM **3** in THF/0.1 M $[NBu_4][CF_3SO_3]$ at T = 238 K. (a) and (b) are CV and rpe scans at 200 and 5 mV/s, respectively, *before* electrolysis. Scan (c) shows rpe *after* exhaustive cathodic electrolysis at $E_{appl} = -2.5$ V (2.0 F/equiv passed); scan (d) is recorded after exhaustive anodic "back-electrolysis" at $E_{appl} = -0.5$ V (1.4 F/equiv passed).

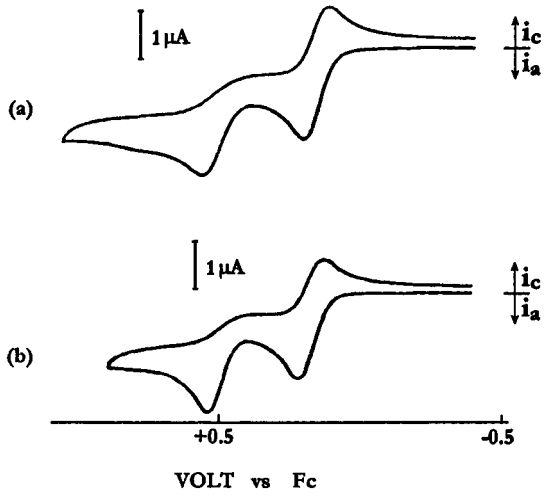

Figure 9. Cyclic (ν = 0.2 V/s) and rotating platinum electrode voltammograms of anodic reactions of 0.42 mM **1** or **2** in CH_2Cl_2/0.1 M $[NBu_4][PF_6]$: (a) complex **1**; note that partial electrode passivation occurs in the rpe scan after the second oxidation process; (b) complex **2**.

of the reduced solution allowed assignment of ν_{CO} for $\mathbf{3}^{2-}$ (Table 4), but the dianions $\mathbf{4}^{2-}$ and $\mathbf{5}^{2-}$ were less stable and could not be confidently assigned.

Some information was obtained about the decomposition products of the dianions from IR and ESR spectroscopy. The IR spectra of reduced solutions of **5** at ambient temperatures demonstrated the presence of $\{[Fe_2(CO)_6S_2]_2Pt\}^{2-}$ (ν_{CO} = 2023, 2000, 1943 cm^{-1})[35] as the major product. Reduced solutions of **3** showed ESR activity for two different Pt-containing radicals, one of which decomposed rapidly, leaving a Pt-containing radical ($\langle g \rangle = 2.045$, $\langle a \rangle_{Pt} = 99 \times 10^{-4}$ cm^{-1}) having a hyperfine interaction with *one* phosphorus atom ($\langle a \rangle_P = 6.7 \times 10^{-4}$ cm^{-1}). These data indicate that scission of $Pt-L_2$ bonds has a role in the decomposition of $[Fe_2(CO)_6S_2PtL_2]^{2-}$, and in the case of $\mathbf{5}^{2-}$, fracture of Pt−S bonds is also likely.

(35) Seyferth, D.; Henderson, R. S.; Song, L. C. *Organometallics* **1982**, *1*, 125.

Oxidations. Complexes **1**−**5** each have a fully reversible one-electron oxidation on the CV time scale in CH_2Cl_2 at room temperature (Table 3, eq 3). These well-

$$Fe_2(CO)_6S_2PtL_2 \rightleftharpoons [Fe_2(CO)_6S_2PtL_2]^+ + e^- \quad (3)$$

behaved waves were followed by a chemically irreversible second one-electron oxidation which sometimes fouled a Pt electrode (Figure 9). An exception was complex **4**, for which the second oxidation was reversible, owing, apparently, to oxidation of the ferrocenyl group. Reduced temperatures were used in bulk electrolyses to generate the monocations. Details of these experiments, including coulometry and examination of the chemical reversibility of eq 3 on a time scale of about 30 min, are summarized in Table 7. The stability of the monocation was in each case sufficient to allow measurement of its IR and ESR spectra (Tables 4−7).

IR spectra of the monocations show the same set of four CO absorptions found for their neutral precursors, but now shifted to appreciably higher energies (Table 5). A minor exception is $\mathbf{4}^+$, which has five CO bands. The average shift of the ν_{CO} energies varies from + 46 cm^{-1} for $\mathbf{3}/\mathbf{3}^+$ to + 76 cm^{-1} for $\mathbf{4}/\mathbf{4}^+$, an average shift of +64 cm^{-1} being observed for the entire set of five complexes. This value is in the range expected for a one-electron change at a dinuclear metal center.[30]

Table 7. Bulk Coulometry for Oxidation of $Fe_2(CO)_6(\mu_3\text{-}S)_2PtL_2$ in CH_2Cl_2 to the Monocation and Recovery of Neutral Complex after Back-Electrolysis

complex	T (K)	E_{appl} (V)	F/equiv[a]	recovery[b] (%)
1	228	0.36	0.8	63
2	233	0.40	1.0	32
3	238	0.38	0.9	83
4	238	0.34	1.1	24
5	233	0.51	1.0	80

[a] Faradays passed in anodic process per equivalent of neutral complex. [b] Calculated from comparison of the plateau rpe current after cathodic re-electrolysis of the monocation ($E_{appl} = 0$ V) with that measured before original anodic electrolysis.

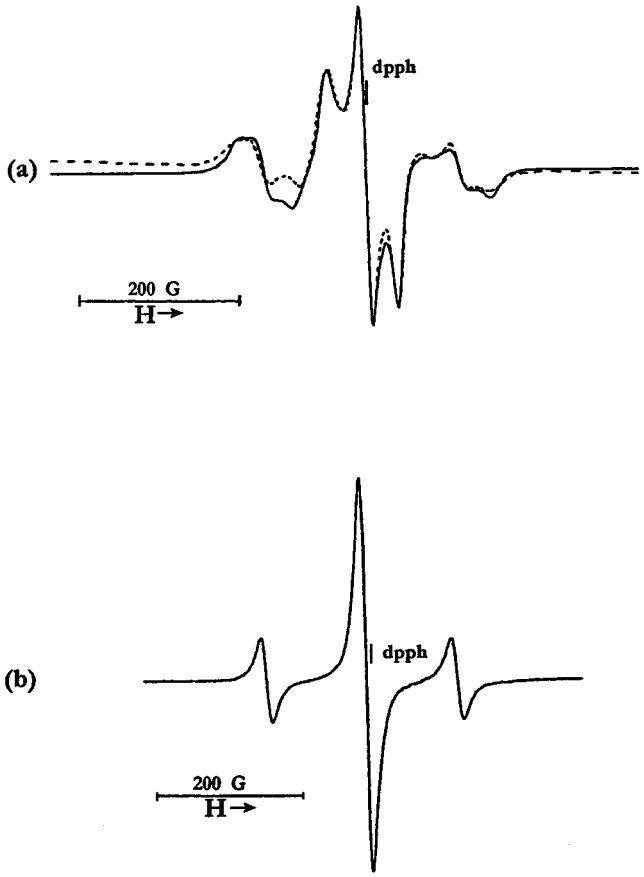

Figure 10. ESR spectra of $\mathbf{1}^+$ recorded after oxidation of ca. 1 mM **1** by equimolar $[(4\text{-}BrC_6H_4)_3N]^+$ at ambient temperature in 1:1 CH_2Cl_2:1,2-$C_2H_4Cl_2$: (a) frozen solution at $T = 77$ K; (b) fluid solution at $T = 223$ K. Resonance of dpph is indicated; solid line is simulation, dashed line is experimental.

ESR spectra were recorded for both frozen solutions and fluid solutions of the monocations with the exception of $\mathbf{5}^+$, for which no frozen spectrum was obtained, and $\mathbf{3}^+$, for which a fluid solution spectrum is lacking. The spectra were generated either by electrolytic oxidation or through reaction with $[(4\text{-}BrC_6H_4)_3N]^+$ in a 1:1 mixture of $CH_2Cl_2/C_2H_4Cl_2$. Each spectrum was successfully simulated (e.g., Figure 10), yielding the parameters of Table 6. Orthorhombic *g*- and *A*-tensors were observed, with *g*-values from about 2.06 to 1.97. Pt hfs were observed in each case, dominated by the isotropic contribution from a low of 126×10^{-4} cm^{-1} for $\mathbf{3}^+$ (calculated from the average of A_1, A_2, and A_3) to a high of 252×10^{-4} cm^{-1} for $\mathbf{2}^+$ (measured in fluid solution). Although these hyperfine values are large in absolute terms, they do *not* necessarily suggest a Pt-localized [i.e., Pt(III)] SOMO. As alluded to above, an isotropic splitting of 200×10^{-4} cm^{-1}, for example, corresponds to only about 1.6% Pt 6s spin density.[36] Genuine Pt(III) complexes generally have much larger Pt hyperfine interactions[37](for example, $[Pt(NO_2)_4]^-$ has an average A_{Pt} of about 2000×10^{-4} cm^{-1}).[37a] The *highly delocalized* square-planar chelate complex $[Pt\{(NH)_2C_2(CN)_2\}]^-$ has an isotropic Pt splitting of about 150×10^{-4} cm^{-1}.[38]

The spectroscopic results are in concert with the EHMO calculations in showing a large change in ν_{CO} upon one-electron oxidation of the Fe_2 center to which the carbonyls are bonded. The Pt spin-density contribution is rationalized on the basis of polarization of the Pt 6s electrons by spin density in the capping S_2 moiety.

Literature Precedents for Reductive Electron-Transfer Sites. The dinuclear complex $Fe_2(CO)_6(\mu\text{-}S)_2$, **6**, which is the prototype for the diiron electron-transfer site in complexes **1**−**5**, has a well-investigated redox chemistry. Seyferth and co-workers reduced this complex with 2 equiv of alkali metal to form the dianion $[Fe_2(CO)_6(\mu\text{-}S)_2]^{2-}$.[39] The dianion is structurally distinguished from the neutral complex by the lack of S−S bonding in the former. That is, two-electron reduction results in cleavage of the S−S bond in $Fe_2(CO)_6(\mu\text{-}S)_2$, suggesting that the LUMO in this dinuclear butterfly complex is antibonding with respect to the S−S interaction.[40] Pickett and co-workers showed[41] that when **6** is reduced by *one* electron in THF (−1.5 V vs Fc), the transient monoanion $\mathbf{6}^-$ dimerizes, giving the previously characterized[42(a)] disulfide-bridged tetranuclear complex $[Fe_4(CO)_{12}S_4]^{2-}$. The dimer can be further reduced (−2.5 V) by two electrons (per dimer) to give $\mathbf{6}^{2-}$,[41] a mechanism subsequently confirmed by Averill and co-workers.[42b] There is, therefore, a basic distinction between the *two-electron* reductions found for the Fe_2S_2 moiety in the clusters **1**−**5** and the *one*- electron reductive chemistry of the Fe_2S_2 group in **6**. In the latter, of course, there is a S−S bond which is lacking in the former. Whether or not this dictates the two different electron stoichiometries is not known, however, since the status of the S−S bond in the monoanion $\mathbf{6}^-$ is unknown.

The two-electron reductive stoichiometry in the clusters is, then, almost certainly due to coupling of electron transfer with making and breaking of the Fe−Fe bond. Reversible metal−metal bond formation is a common cause of two-electron stoichiometries in dinuclear complexes[43]and has a direct precedent for dinuclear Fe_2 complexes in the reduction of $Fe_2(CO)_6(\mu\text{-}PPh_2)_2$, which

(36) An unpaired electron localized in the 6s orbital of ^{195}Pt has a theoretical hyperfine splitting (see ref 31) of over 10^4 G.

(37) (a) Wermeille, M.; Geoffroy, M.; Arrizabalaga, P.; Bernardinelli, G. *Inorg. Chim. Acta* **1993**, *211*, 81. (b) Uemura, T.; Tomohiro, T.; Hayamizu, K.; Okuno, Y. *Chem. Phys. Lett.* **1987**, *142*, 423. (c) Nizova, G. V.; Serdobov, M. V.; Nikitaev, A. T.; Shul'pin, G. B. *J. Organomet. Chem.* **1984**, *275*, 139. (d) A leading reference for Pt(III) complexes is: Woolins, J. D.; Kelly, P. F. *Coord. Chem. Rev.* **1985**, *65*, 115.

(38) Senftleber, F. C.; Geiger, W. E. *Inorg. Chem.* **1978**, *17*, 3615.

(39) Seyferth, D.; Kiwan, A. M.; Sinn, E. *J. Organomet. Chem.* **1985**, 281, 111.

(40) Weatherill, T. D.; Rauchfuss, T. B.; Scott, R. A. *Inorg. Chem.* **1986**, *25*, 1466.

(41) Al-Ani, F. T.; Pickett, C. J. *J. Chem. Soc., Dalton Trans.* **1988**, 2329.

forms the corresponding dianion in a single two-electronvoltammetric wave.[44]

In clusters **1** and **2**, reduction of the Pt(II) site precedes reduction at Fe_2S_2. There is ample precedent for this process in the behavior of (π -diimine)Pt(II)L_2 complexes. For example, the one-electron reductions of $[(bpy)Pt(PMe_3)_2]^{2+}$,[32] (bpy)Pt(mesityl)$_2$,[33] and the platinacycle (bpy)Pt(C_3H_6)[45] are all reversible one-electron processes giving a radical with spin localized primarily on the bipyridyl ligand. Isotropic Pt hfs in the range $(40-55) \times 10^{-4}$ cm^{-1} are common for these systems, in agreement with the values found for $\mathbf{1}^-$ and $\mathbf{2}^-$.

Summary

1. The basic redox chemistry of the cluster compounds $Fe_2(CO)_6(\mu_3\text{-}S)_2PtL_2$ involves a two-electron reduction and a one-electron oxidation of the neutral complex. In the case wherein L_2 has a low-lying π^* orbital, a second (one-electron) reduction is observed at potentials positive of the two-electron process. The one-electron and two-electron sites are, to some extent, independent of each other, as shown by IR and ESR measurements on the resulting anions and polyanions.

2. Precedent for the two-electron process is most direct in the reduction of $Fe_2(CO)_6(\mu\text{-}PPh_2)_2$, in which Fe−Fe bond cleavage accompanies the formation of the corresponding dianion.[44] This analogy is superior to that associated with the reduction of $Fe_2(CO)_6(\mu_2\text{-}S)_2$, which occurs in two well-separated one-electron steps.[41,42] The dianion $[Fe_2(CO)_6(\mu_2\text{-}S)_2]^{2-}$ retains its metal−metal bond and undergoes, instead, S−S cleavage, a process repeated in homologues having Se or Te bridges.[39,40] The energetically more facile process for clusters **1**−**5** is, apparently, scission of the Fe−Fe bond.

Acknowledgment. This work was supported at the University of Vermont by the National Science Foundation (CHE 94-16611 and CHE 97-05763) and at the Texas universities by the Robert A. Welch Foundation (B-1093 to M.G.R. and P-074 to W.H.W.).

Supporting Information Available: Listings of crystallographic data, bond distances, bond angles, and positional parameters for $Fe_2(CO)_6(\mu_3\text{-}S)_2Pt$(phen) and $Fe_2(CO)_6(\mu_3\text{-}S)_2$-Pt(cod). This material is available free of charge via the Internet at http://pubs.acs.org.

OM010838A

(42) (a) Bose, K. S.; Sinn, E.; Averill, B. A. *Organometallics* **1984**, *3*, 1126. (b) Barber, D. E.; Sabat, M.; Sinn, E.; Averill, B. A. *Organometallics* **1995**, *14*, 3229.

(43) Collman, J. P.; Rothrock, R. P.; Finke, R. G.; Moore, E. J.; Rose-Munch, F. *Inorg. Chem.* **1982**, *21*, 146.

(44) Ginsburg, R. E.; Rothrock, R. K.; Finke, R. G.; Collman, R. G.; Dahl, L. F. *J. Am. Chem. Soc.* **1979**, *101*, 6550.

(45) Klingler, R. J.; Huffman, J. C.; Kochi, J. K. *J. Am. Chem. Soc.* **1982**, *104*, 2147. This paper also discusses the reduction of the Pt(II) complex Cl_2Pt(bpy), which is similarly investigated in a later paper by: Yang, L.; Wimmer, F. L.; Wimmer, S.; Zhao, J.; Braterman, P. S. *J. Organomet. Chem.* **1996**, *525*, 1.